CNRS
Centre National de la Recherche Scientifique

INFN
Istituto Nazionale di Fisica Nucleare

Analysis of antropic seismic waves at the Virgo site

VIR-0303A-12

A. Cesarini, I. Fiori and B. Swinkels
EGO - European Gravitational Observatory, Pisa, Italy

Issue: 1

Date: September 8, 2012

VIRGO * A joint CNRS-INFN Project
Via E. Amaldi, I-56021 S. Stefano a Macerata - Cascina (Pisa)
Secretariat: Telephone (39) 050 752 521 * FAX (39) 050 752 550 * Email W3@virgo.infn.it

Contents

1 Introduction

Previous studies of ground seism at EGO observatory demonstrated the presence of correlated behavior between the Virgo dark fringe and the seismic data [2]. However, very efficient 'superattenuators' have been designed for the Virgo interferometer. Contributing to isolate the Virgo Test Masses, they increase the robustness against the perturbations provoked by seismic waves [1], there are still evidences that ground seisms perturb the dark fringe. A mechanism to be mentioned in this respect, relates the production of diffuse light [3]. However, several interferometer devices are not suspended to the superattenuators and, thus, seismic waves can still perturb the interferometer response introducing noise [2].

Historically, one of the most significant contribution at the origin of the antropic seismic noise (with particular emphasis between $1 - 4$ Hz) was observed for transients of about $30 - 40$ s with 24 h modulation (with a minimum around 1:00 AM) and reduced activity during the week ends. Figure 1 shows the surroundings of the EGO observatory and the location of viaducts considered to be the most likely emitters of antropic ground seisms in the $1 - 4$ Hz band [4]. Viaducts and bridges are located at distance from 1 to 3 km from the Virgo corners and terminal experimental areas.

In the present work, we identified the most likely southern incoming direction of antropic seismic waves at the Virgo site (roughly at the B2 position, see Figure 1).

2 Data taking strategy

The Guralp CMG-40T (or G40T), placed inside the central building (CB, LAT: 43° 37′ 53.08", LON: 10° 30′ 16.1885") is part of the vibrational monitoring array at the Virgo observatory. The Guralp Systems CMG-40 instruments are rugged and robust triaxial (Z, N, E) broadband seismometer ideally suited for installation in vaults with moderate noise. It has a response of 30 s at 50 Hz standard with a lowest spurious resonance measured at 450 Hz and no self-noise adding. The G40T output is sampled at 1000 Hz and later decimated at 250 Hz (bringing ±0.06 s of uncertainty in the time-domain). We also utilized a mobile Guralp CMG-3T (or G3T) that, basing on our observation scheduling, has been placed beside the G40T for cross-calibration (Huddle test) and at the OvoBettini S.R.L. (LAT: 43° 37′ 22.87", LON: 10° 30′ 28.27" [coordinates derived from GoogleEarth]) for data taking. The G3T is widely used on many national seismic networks being a compact triaxial (Z, N, E) broadband sensor suitable for surface, subsurface and borehole vaults. It is provided with built-in digitizer (250 Hz sampling frequency), acquisition module, storage and communication devices [5]. Both the Guralp devices possess an almost identical response in the 0.1-100 Hz band. In the present work we will use only the vertical (Z) component of the recorded dataset.

3 Two-seismometer setup and reconstruction technique

The adoption of only two seismometers drastically reduces the investigation capability. In fact, using only two seismometers, it is not possible to univocally identify the origin of the seismic waves. For incoming (plane front) waves, it is only possible to compute the time delay t measured as the detection time difference of a seismic wave passing at the location of the two seismometers. The time delay quantification provides information for identifying the wave arrival direction. Unfortunately, in the case of adopting only two seismometers, for any detected wave, they exist two possible arrival directions (Figure 7)

However, providing an estimation of the wave propagation speed $v = 1/w$, where w is the complementary slowness factor, we are able to identify the two possible arrival directions associated with the incoming seismic waves. Then, the wave time delay $t = d/v$ is related to the direction angle α of the incoming (plane front) wave as in the equation below:

$$\alpha = arccos(d/D) \tag{3.1}$$

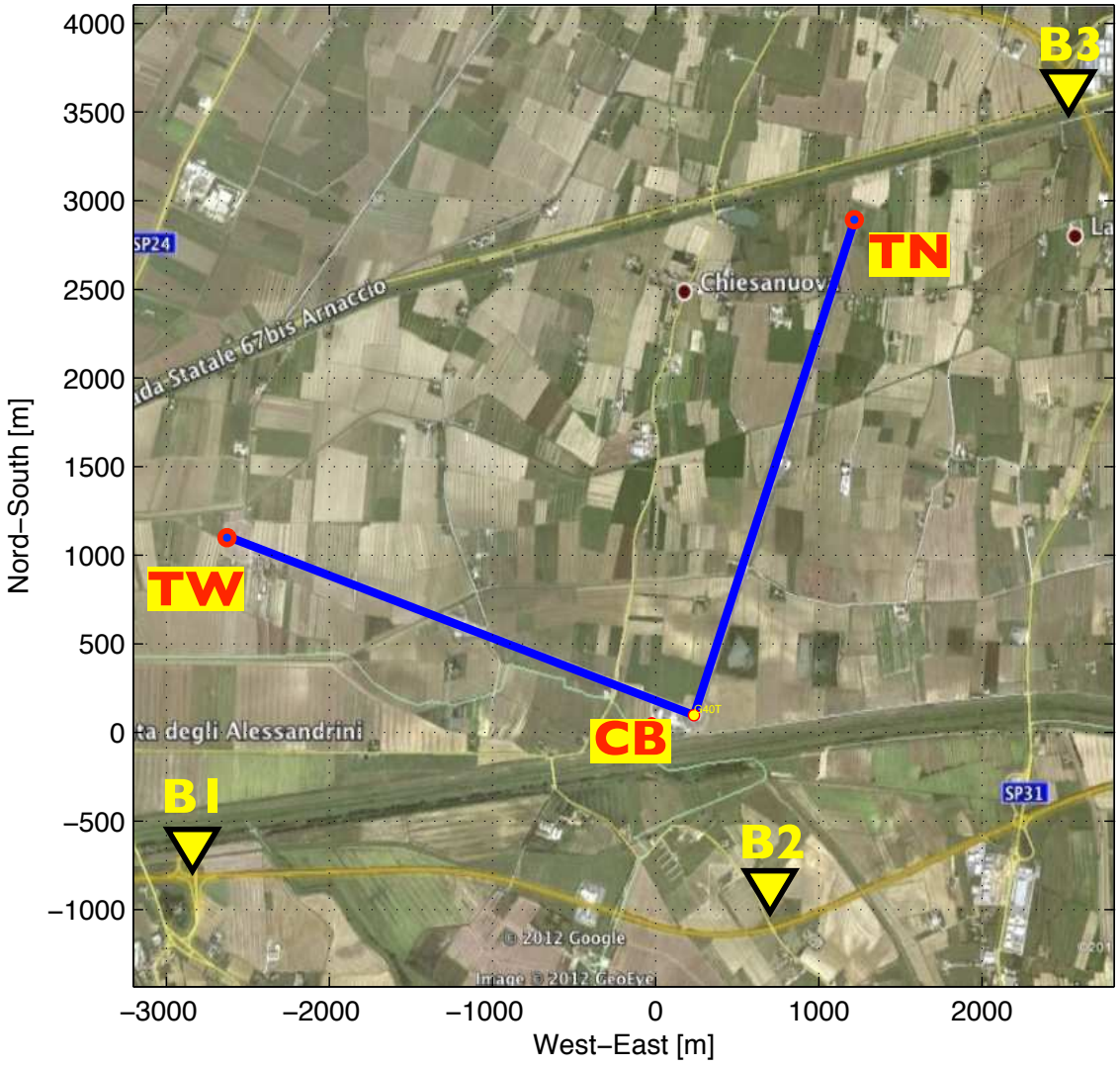

Figure 1: Locations of the three closer locations at which antropic seismic waves around the Virgo site might be originated: B1 (SS-206 national road), B2 (Fi-Pi-Li highway) and B3 (road SP31). The Virgo 3 km arms are also shown in the map (blue). Also, the locations of the central building (CB) and the north and the west towers (TN and TW, respectively) are drawn (yellow-red circles).

where d is the length of the seismic wave propagation in the time t and α is the angle between the line joining the two seismometers, the D segment, and the arrival direction of the detected wave fronts at the two seismometer locations.

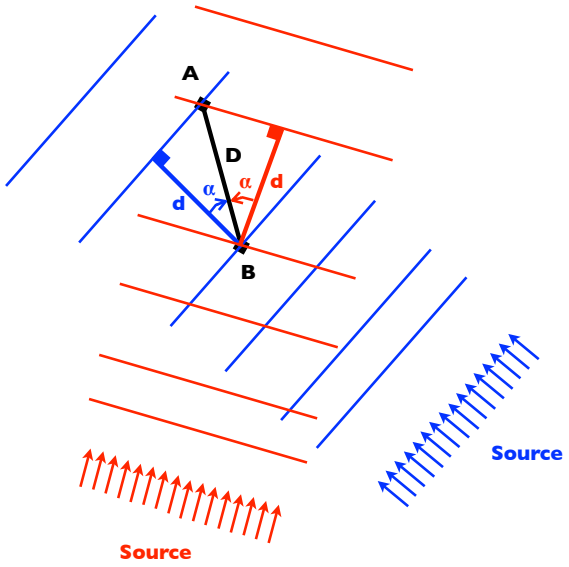

Figure 2: Two-seismometer singularity configuration (under the plane wave assumption).

The quantification of the α angle depends on the determination of the wave propagation speed v that is frequency dependent and varies for different soil characteristics. In 2009, the sedimentary nature of the soil layers surrounding the Virgo site was already identified [9]. At the time of such a study, the soil was highly saturated of water and the superficial seismic wave bulk speed was estimated to be within $150-200$ m between $1-5$ Hz [10]. This result was in agreement with the other more comprehensive and generalized studies results investigating different concentrations of water in the soil layers [8]. Therefore, during July and August 2012, the soil can be effectively considered as completely dry. This leads to adopt a correction factor on the bulk speed of $\simeq 1.5$ [8] that brings the bulk surface wave speed nearby the Virgo site, within the $v = 225-300$ m/s interval. However, in past dedicated studies carried out at the Virgo site provided an estimation of $280-430$ m/s ($1-4$ Hz) in presence of moderately content of water in the soil ($\sim 1-10$ m below the ground) [4] and 368 m/s ($\simeq 2.35$ Hz) [7] for dry soil. Thereby, we choose to adopt the conservative estimate for the wave speed range of $325-425$ m/s in the $2-5$ Hz band.

4 Huddle tests for seismometer intercalibration

We set a preliminary procedure to carry out the temporal and spectral response intercalibration between the G40T and the G3T seismometers before data taking [5]. This procedure is commonly referred as a Huddle test. After the measurements, we produced further Huddle tests assessing whether the identified intercalibration parameters were reliable. In order to achieve such as cross-calibration, we placed the G3T and the G40T side by side in the CB at ground level in proximity with the interferometer beam splitter. Then, we recorded several hours of seismic data. During daytime, the frequency response of the two seismometers was stressed by the seismic perturbation of antropic origin produced by the manual workers at the site. The seismic waves provoked via mechanical solicitations provided the temporal marks that helped in correlating the two datasets recorded by the G3T and the G40T along their whole operative frequency band. Being connected with the GPS receiver, the G40T is constantly aligned with the GPS time. The direct comparisons of the wave arrival times shown that, in the last ~ 4 years of operation, the G3T has experienced a significant temporal shift from the GPS

time[1]. Confirmed for each of the nine 2-hour runs of observation, via correlation analysis, we quantified their temporal offset in +392.42 s. Finally, after the resynchronization, the two seismometers resulted correlated at lag zero (see Figures 3).

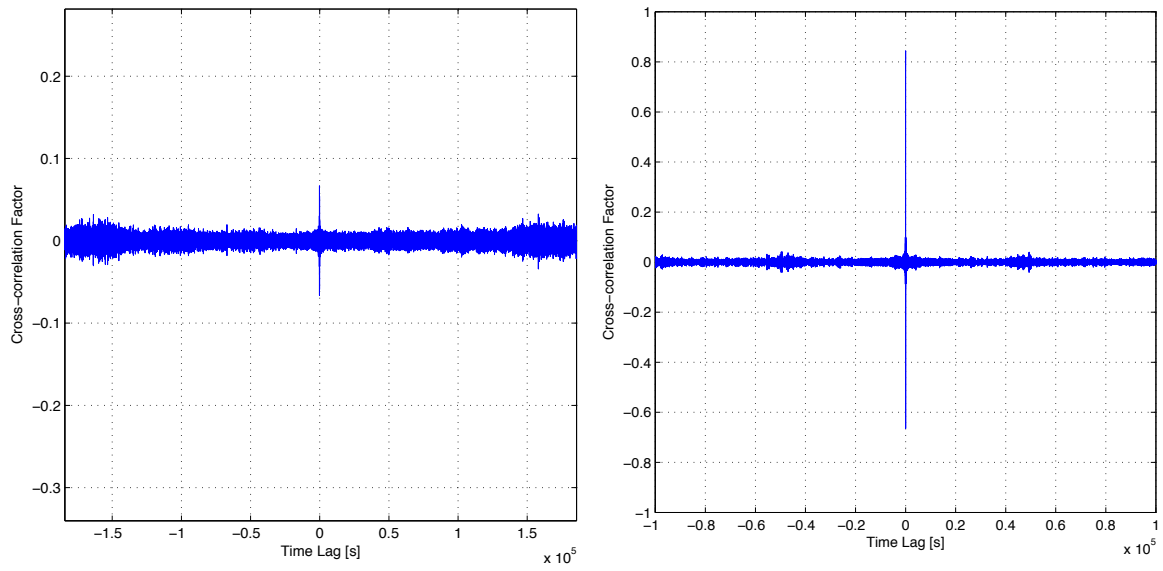

Figure 3: After the calibration procedure the two seismometer clocks are perfectly synchronized. (Left) G3T vs. G40T cross-correlation showing a relatively significant correlation factor at lag zero ($\rho = 0.07$) with data filtered in the $1 - 15$ Hz band. (Right) For data filtered in the $1 - 8$ Hz band, the correlation factor increases dramatically obtaining $\rho = 0.83$. The correlation factors are normalized in the range between -1 and 1.

We carried out a second and a third Huddle test (after two and 5 weeks). We used this new sets of data to model the shifting time factor that the G3T experiences against the GPS time. The modeling consists in a linear interpolation of the correlation results obtained analyzing the whole intercalibration dataset (Figure 4), obtaining:

$$t_{G40T} \equiv t_{GPS} = a \cdot t_{G3T} - T0 \tag{4.1}$$

with $a = 0.48$ and $T0 = 392.42$ s (with fitting residuals 0.04 s).

Due to their slight different characteristics, G40T and G3T produce a small divergence in their spectral responses for $f > 20$ Hz. Thereby, by introducing a low-pass filtering, we discarded their spectral components outside the interval $0 - 20$ Hz obtaining a very remarkable correspondence of their power spectral density (PSD) behaviors (Figure 9).

However, we suggest that a continuous realignment of the G3T internal clock with the GPS signal would solve the issue related to the time shifting. Unfortunately, the seismometer GPS antenna is not working properly. Thereby, in the near future, we are planning to fix or replace this device in the attempt to regain the G3T full capability.

[1]Likely, this delay should be ascribable to the oscillator circuit or, more likely, related with the unreliability of internal battery pack reference voltage.

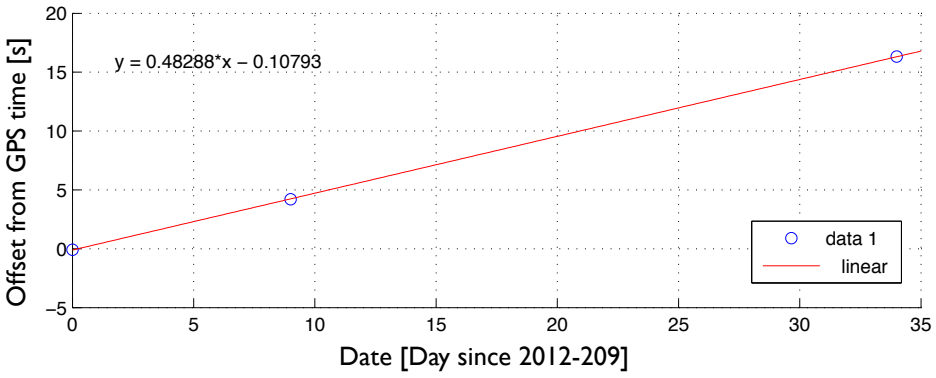

Figure 4: Modeling of the G3T internal clock versus GPS temporal shift.

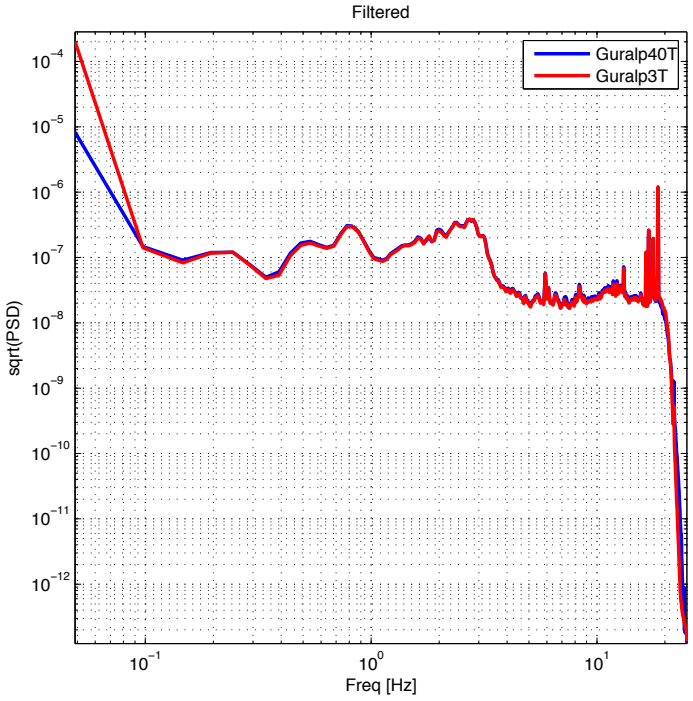

Figure 5: In the $0 < f \leq 20$ Hz band, the seismometer spectral responses are, in practice, identical.

5 Investigation of the seismic noise from the southern direction

We recorded a total of 8 hours of observation. As first data validation step, we estimated from the datasets their information related to the microseism component. The microseism is a seism associated with the sea activity that has $v > 1$ km/s from the western direction [9]. The two seismometers are aligned almost in the south direction. Thus, the time lag between the G3T and the G40T recorded time-series must be very very small. In fact, as expected, the microseism produces a significant correlation factor at lag zero (see Figure 6).

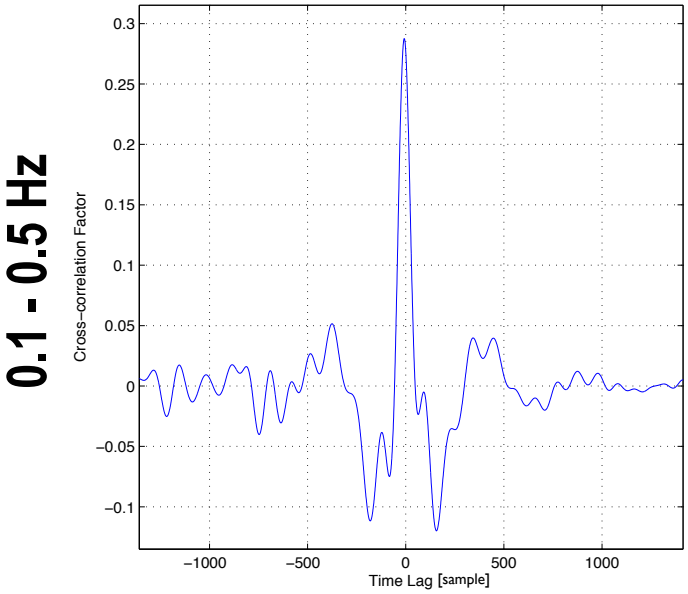

Figure 6: Microsiesm waves due to sea that interact mechanically with the continental plate.

The identified modulation of seismic waves of antropic origin is based on a 24-hour period and the reduced activity during the week ends dragged the search for their origins toward the moderately traffic populated highways and roads around the Virgo site [4]. Placing the G3T seismometer close to the S.G.C. Fi-Pi-Li (southern highway, see Figure 7) at OvoBettini S.R.L. farm location, we obtained measurements of the antropic seismic waves emitted from this southern highway. If emitted at that locations, the antropic seismic waves should be transiting, first, the G3T position and later, after experiencing an attenuation at higher wavelengths along their $\simeq$1059 m path toward the Virgo site, they should be detected again by the G40T placed inside the CB.

Unremarkably, the human and the machine activity at the OvoBettini S.R.L. location produced extended periods of superimposed noise at any wavelength up to, at least, 25 Hz. However, we were able to select a continuous observation of 4600 s in which the noise shown a very significant decrease in the $1-15$ Hz band (Figure 8) in which we selected the signals introducing a pass-band filter. At the same time, inside the CB also, the G40T recorded a reduced activity of mechanicals and manual workers.

Estimating the time lag of the seismic waves of antropic origin, we computed the cross-correlation factors between the two (vertical) Z-component time series of the recorded datasets [5]. The component of antropic seismic waves coming from the southern highway should be contained in the $1-5$ Hz frequency interval [4]. We split the seismometer responses in two relatively $1-8$ Hz and $5-13$ Hz broad bands with $\simeq 40\%$ overlap in frequency (Figure 10). The analysis in the $1-8$ Hz band clearly returned a relatively high correlation factor ρ of about 0.10 peaking on a signal variance of $\cong 0.01$, while the analysis in the $5-13$ Hz band returned significantly smaller correlation values.

Moreover, we further subdivided the $1-8$ Hz band response in 7 subbands ($1-3$ Hz, $2-4$ Hz, $3-5$ Hz,

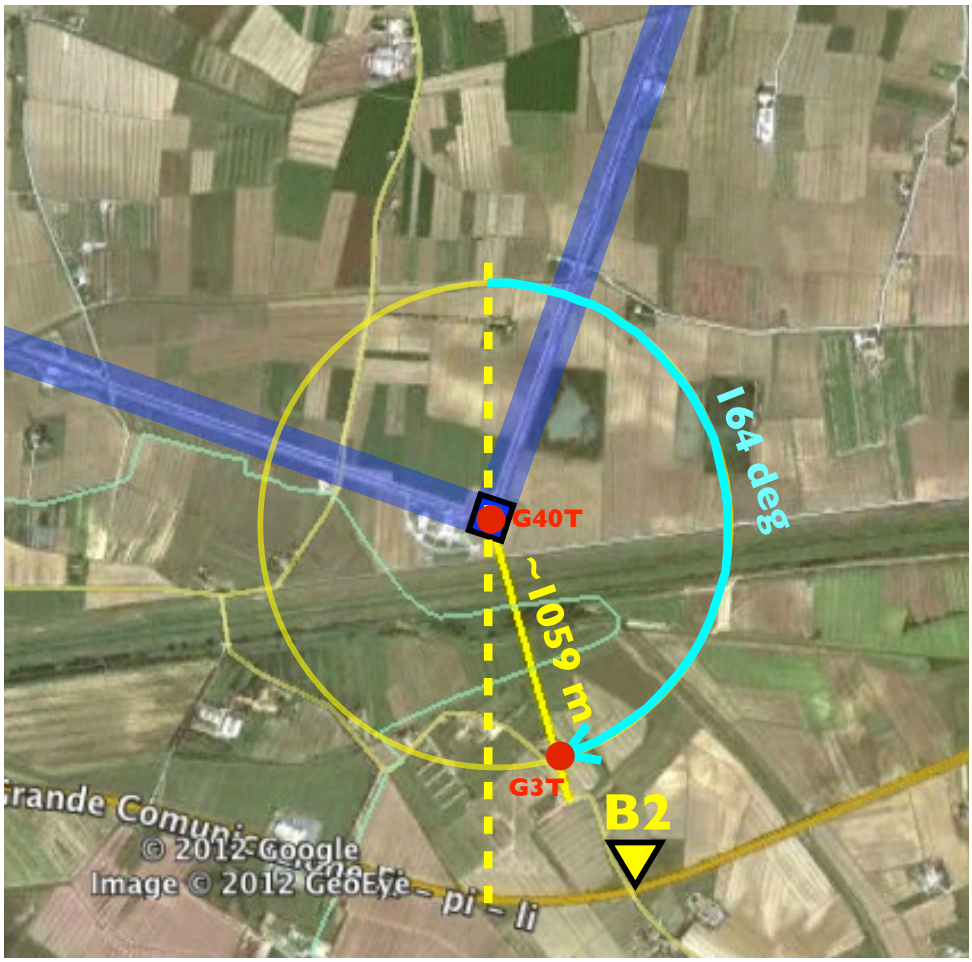

Figure 7: Configuration of the seismometer setup consisting in the G40T placed inside the CB at $\simeq$1059 m from the G3T that was relocated at OvoBettini S.R.L. The azimuthal angle (measured clockwise from the geographic North direction) of the setup is $\simeq$164 deg.

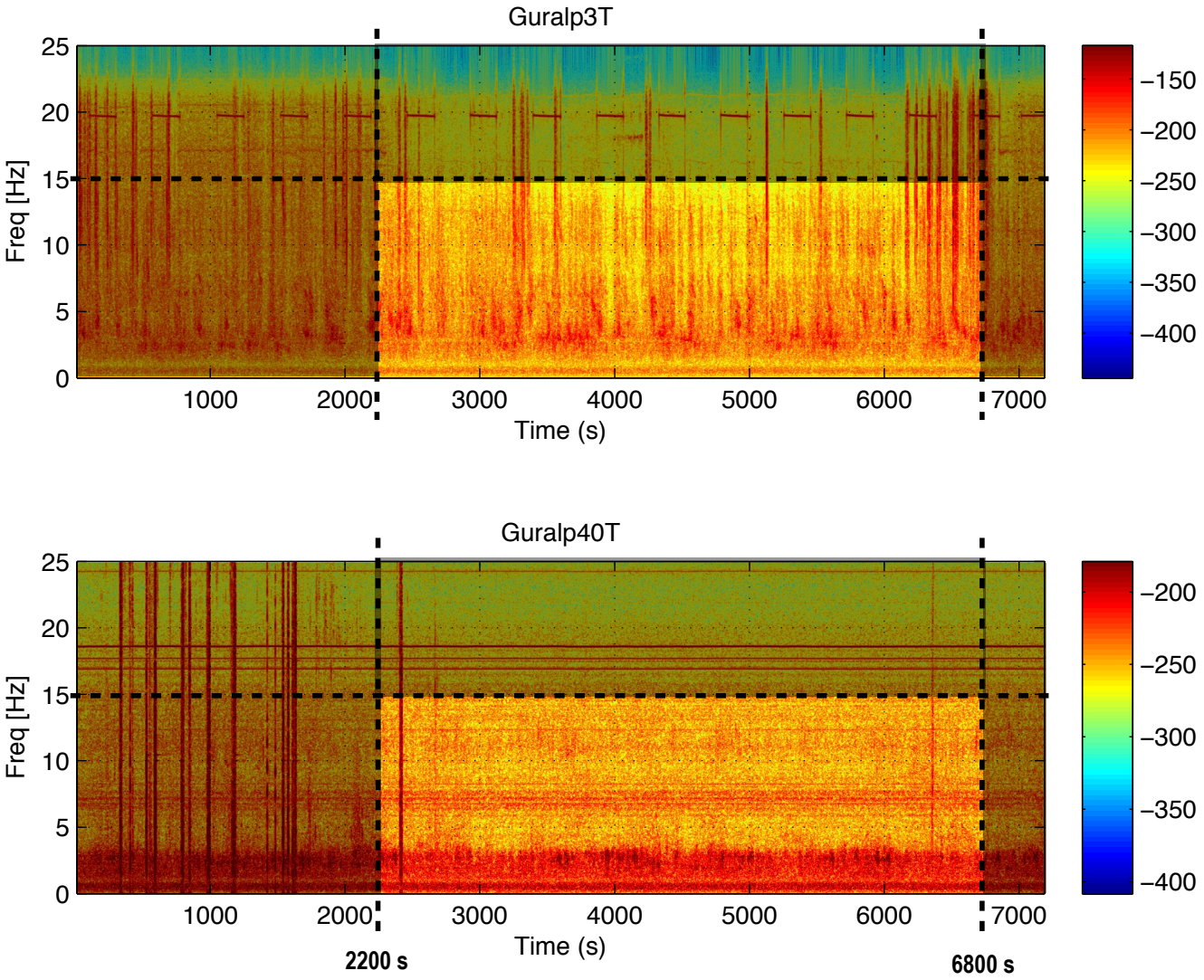

Figure 8: Spectrogram of the data recorded at OvoBettini S.R.L. location (about $\simeq$ 1059 m from the CB).

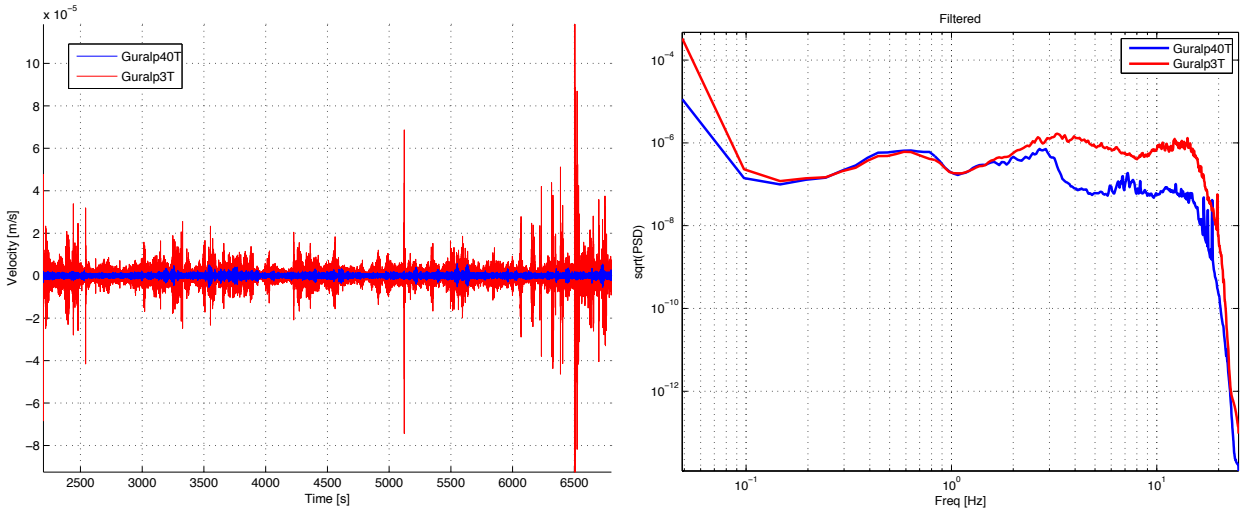

Figure 9: (Left) Time-domain plot of the selected portion of datasets ($\sim$4600 s). The G40T was place inside the CB and the G3T was relocated at OvoBettini S.R.L. farm at about $\simeq$1059 m from the CB. (Right) Ground velocity spectral amplitude measured by the G40T and G3T filtered in the $1 \leq f \leq 15$ Hz band between $2200 \leq t \leq 6800$ s.

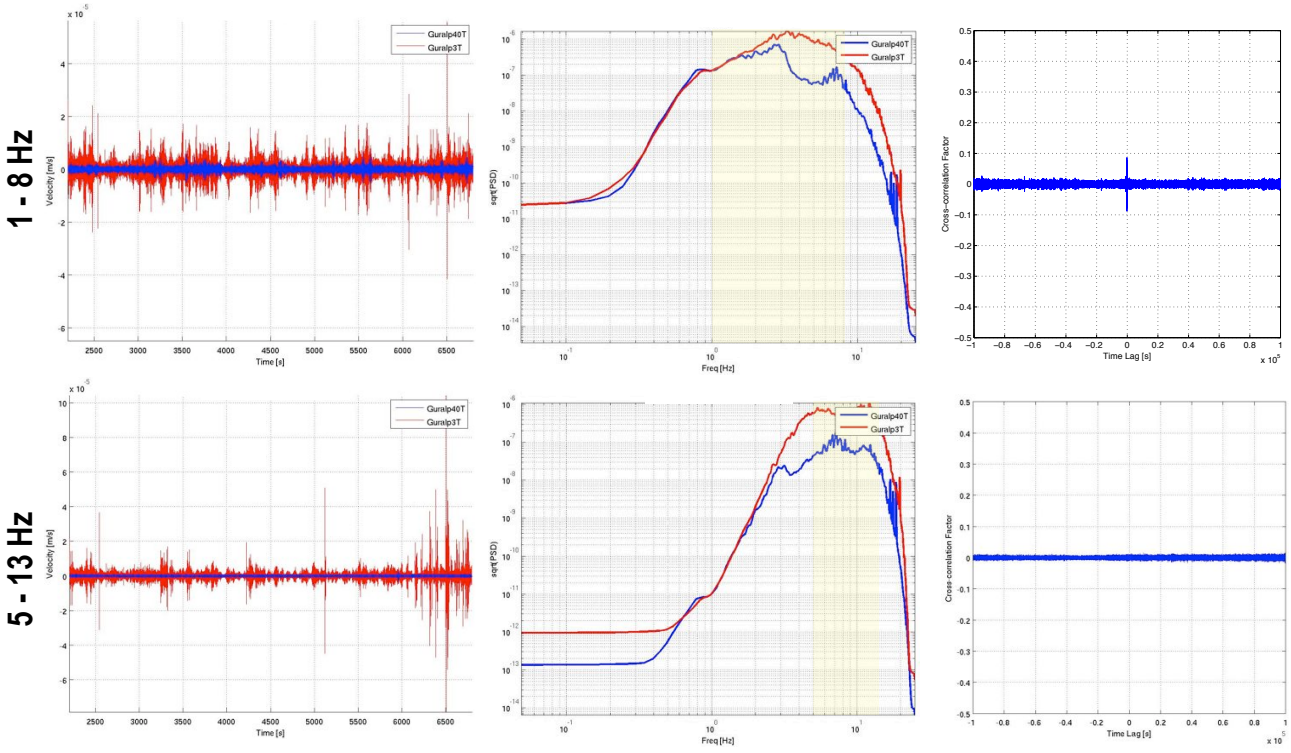

Figure 10: Two frequency split results with frequency overlapping window of $\simeq$40% in frequency.

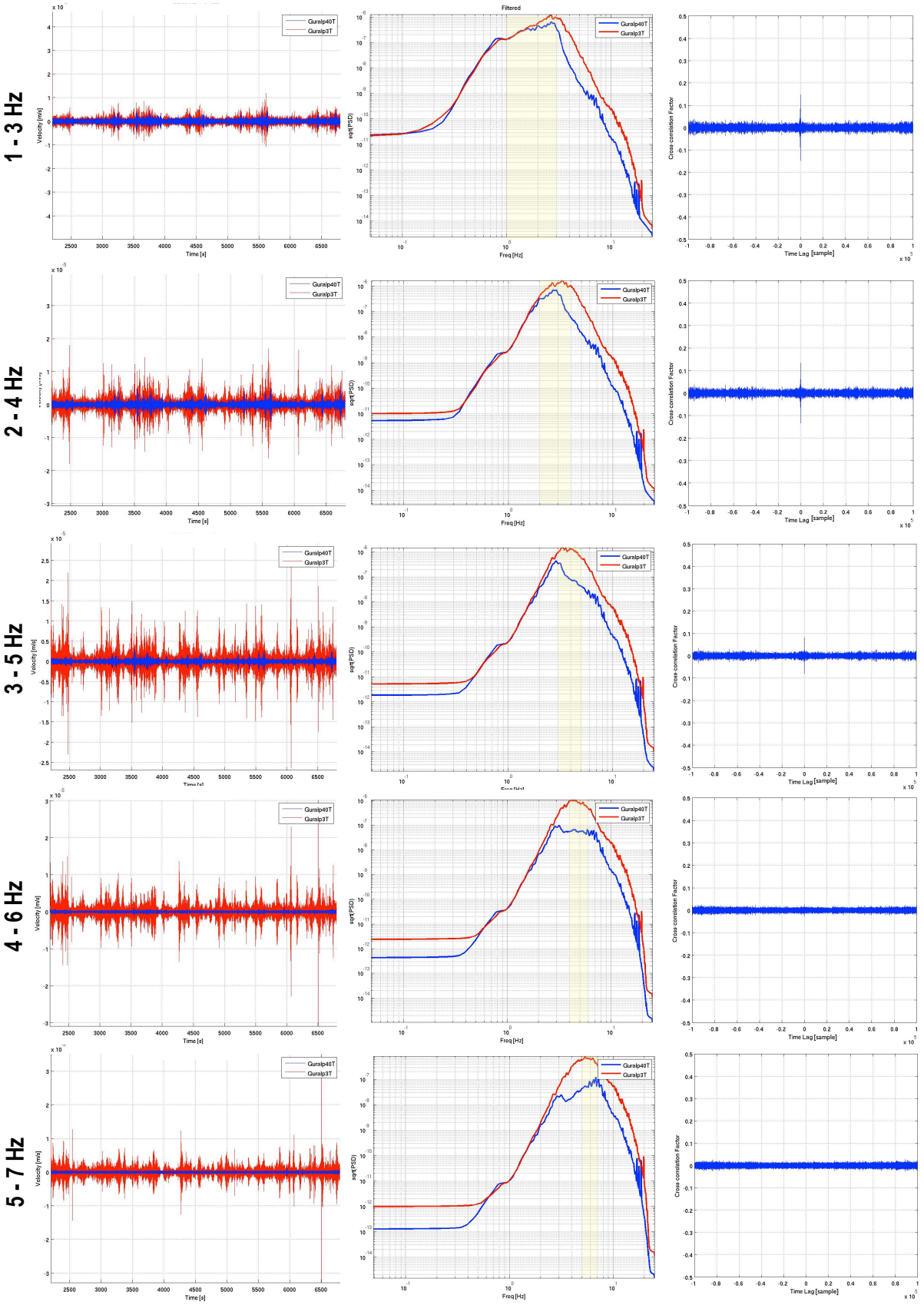

Figure 11: Spectral subinterval division results adopting a 50% frequency overlapping window.

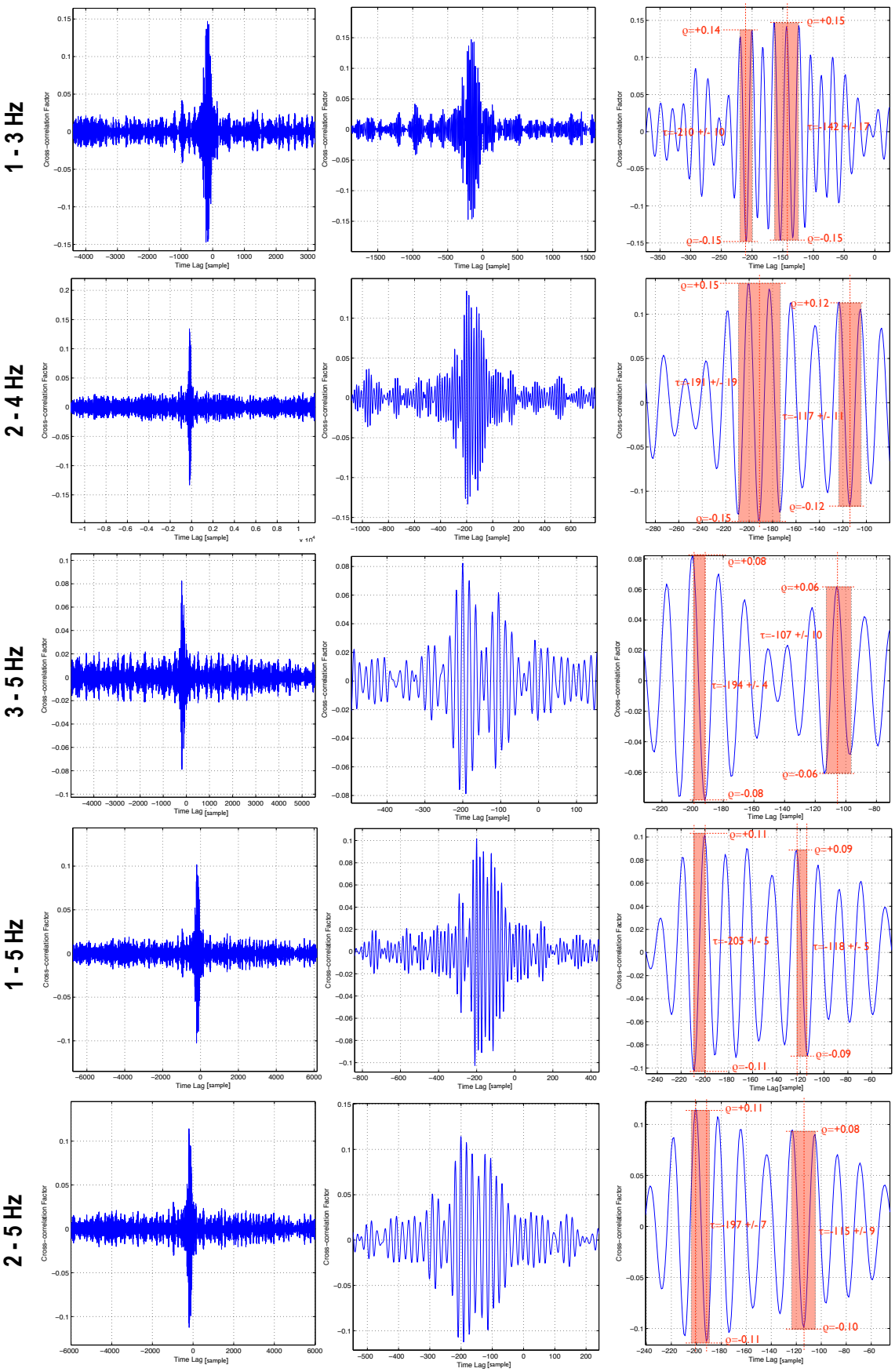

Figure 12: Magnification on the cross-correlation delay of the antropic seismic waves coming from the south of the Virgo site.

$4-6$ Hz, $4-7$ Hz, $1-5$ Hz, $2-5$ Hz) with an overlap of 50% in frequency for the first five subbands (see Figures 10, 11 and 12).

We obtained significant correlation factors[2] ρ contained between 0.08 and 0.15 peaking on a variance plateau of a factor of maximum 0.02 in the $1-3$ Hz, $2-4$ Hz, $3-5$ Hz, $1-5$ Hz and $2-5$ Hz bands. The existence of a cross-correlation in these different bands confirms that such correlation was not obtained by chance but it relates a real content of information the recorded datasets. Also, negative values of time lags corresponds to antropic seismic waves irradiated closer to the G3T than to G40T. In any band, we obtain two different significant time lags at $\sim$120 samples and $\sim$200 samples. Excluding the correlation results obtained in the $1-3$ Hz band in which it seems present a lower SNR, the time lag obtained in the other bands agree with values around $\cong 115 \pm 9$ samples.

Since the propagation speed of seismic waves is frequency dependent, the filtering selects a bunch of waves that, following the same path, arrives at the seismometer locations with slight different times. Also, the information of the propagation of the superficial seismic waves along the minimum path length should be returned by the minimum time-lag values. For time-lag values around $\cong 115 \pm 9$ samples, considering the sampling frequency $F_s = 50$ Hz, we obtained a correlation lag between the two seismometers of $\cong 2.30 \pm 0.20$ s. However, because the continuous shift between the two seismometer clocks, we need to compensate for the continuous time shifting of the two seismometer clocks (quantified carrying out several Huddle tests) and the data taking at the OvoBettini S.R.L. that consists in 0.38 ± 0.05 s. The corrected time-lag estimate $t_{delay} \cong 1.92 \pm 0.21$ s returns the direction angles $\alpha_{min} = 32.6°$ for $v = 325$ m/s and $\alpha_{max} = 57.7°$ for $v = 425$ m/s, respectively (see Figure 13).

6 Conclusion

Due to the significant uncertainty assumed on the wave speed in the lower part of the band (if $v = 325 - 425$ m), we are not able to precisely identify a direction, but a range of incoming directions. Since we adopted only two seismometers, this solutions return two angular sectors crossing the G.S.C. FI-PI-LI highway in two distinct segments. However we selected the south-east cone of solutions that is oriented in the direction of the S.G.C. Fi-Pi-Li where it is present an extended viaduct. It is plausible to consider that the intense transient(s) might be originated by trucks hitting the viaduct junctions (see Figure 14). Concluding, with the present analysis, we identified and constrained the segment of the viaduct where, most likely, the antropic seismic waves are originated.

References

[1] S. Braccini, *et al.* 2005 *Measurement of the seismic attenuation performance of the VIRGO*, Astroparticle Physics 23 (2005) 557-565. 2

[2] I. Ferrante *Seismic contribution to dark fringe signal during E3*, VIR-NOT-PIS-1390-226 (2002) 2

[3] T. Accadia *Noise from scattered light in Virgo's second science run data*, Class. Quantum Grav. 27 (2010) 2

[4] I. Fiori, L. Holloway and F. Paoletti *Studies of the 1-4 Hz seism*, VIR-NOT-FIR-1390-251 (2003) 2, 4, 7

[5] V. Boschi and A. Gennai *Guralp CMG-3TD and CMG-AEM Quick Guide*, VIR-0172A-10 (2010) 2, 4, 7

[6] E. Marchetti, M. Mazzoni and M. Ripepe *Low frequency seismic wave-field array analysis at Virgo*, VIR-NOT-FIR-0281C-12 (2002)

[7] E.G. Beker *Seismic correlation measurements at the Virgo site*, VIR-NOT-FIR-na-na (2012) 4

[2] Correlation factors normalized between -1 and 1.

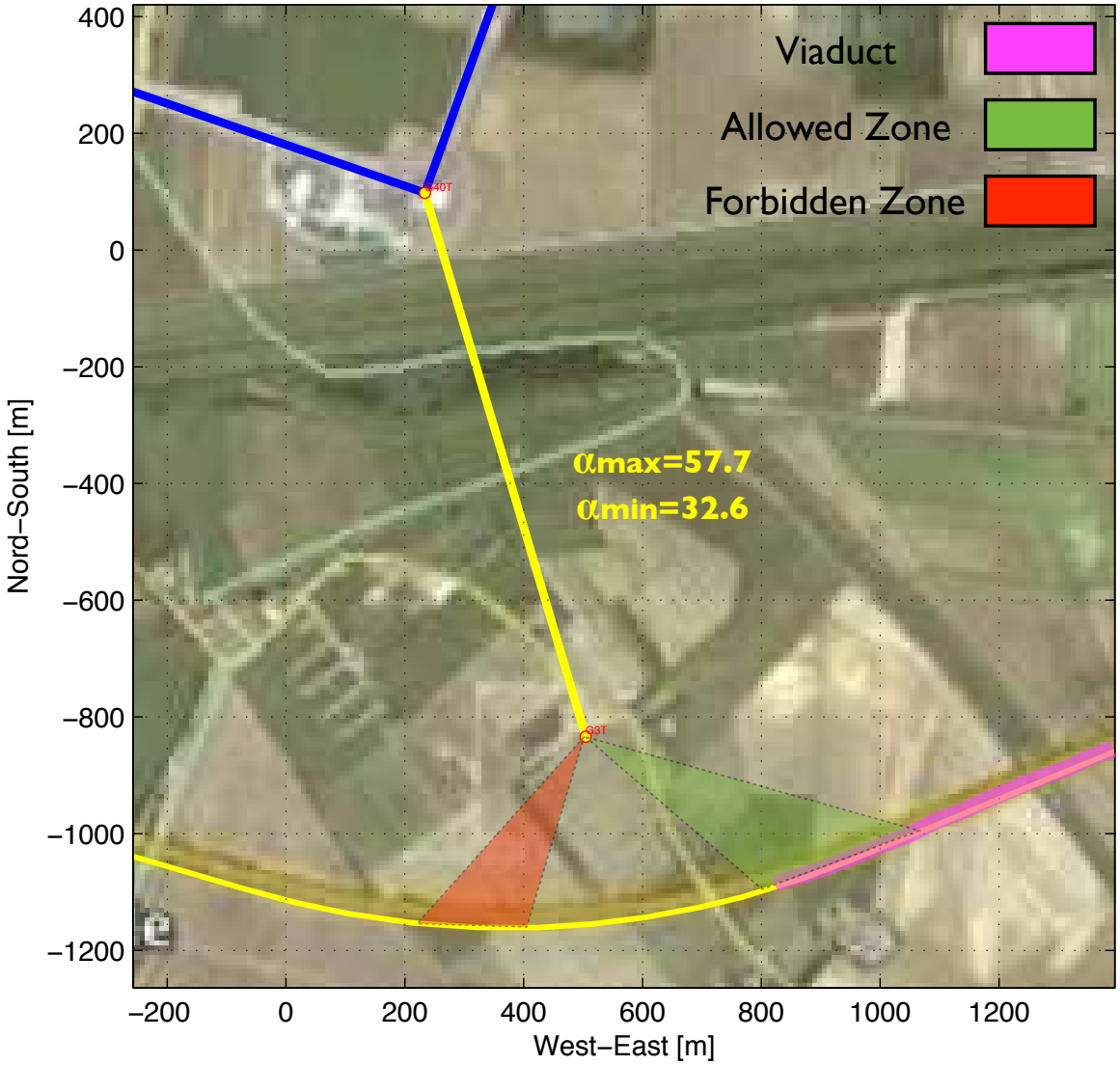

Figure 13: Angular sectors (red and green) identified from the results of the analysis ($\alpha_{min} = 32.6°$ for 325 m/s and $\alpha_{max} = 57.7°$ for 425 m/s). It is also highlighted the segment of the G.S.C. FI-PI-LI highway consisting in a viaduct (magenta) close to the Virgo site.

Figure 14: Snapshot of one of many viaduct junctions hit at the passage of trucks. The junctions are the most likely origins of the antropic seismic waves reaching the Virgo site from the southern direction (in the picture at the extreme right).

[8] J.P. Castagna, M.L. Batzle and R.L. Eastwood *Relationship between compressional-wave and shear-wave velocities in clastic silicate rocks*, Geophysics, Vol. 50, NO. 4 (April 1985): P 571-581 FIGS, 2 TABLES 4

[9] G. Soccorrotti, D. Piccinini, L. Cauchie and I. Fiori *Guralp CMG-3TD and CMG-AEM Quick Guide*, Virgo Paper (2010) 4, 7

[10] G. Soccorrotti, D. Piccinini, L. Cauchie, R.M. Azzara, T. Braun and N.P. Agostinetti *Misure di rumore sismico nei dintorni dell'antenna interferometrica VIRGO (Cascina, Pisa)*, Convenzione Virgo-INVG (2010) 4